A Journal of the Gesellschaft Deutscher Chemiker

Angewandte International Edition GDCh Chemie

www.angewandte.org

Accepted Article

Title: Ag44(EBT)26(TPP)4 Nanoclusters with Tailored Molecular and Electronic Structure

Authors: Taeghwan Hyeon, Megalamane S. Bootharaju, Sanghwa Lee, Guocheng Deng, Sami Malola, Woonhyuk Baek, Hannu Häkkinen, and Nanfeng Zheng

To be cited as: *Angew. Chem. Int. Ed.* 10.1002/anie.202015907

Link to VoR: https://doi.org/10.1002/anie.202015907

WILEY-VCH

10.1002/anie.202015907

WILEY-VCH

RESEARCH ARTICLE

$Ag_{44}(EBT)_{26}(TPP)_4$ Nanoclusters with Tailored Molecular and Electronic Structure

Dr. Megalamane S. Bootharaju[+], Sanghwa Lee[+], Guocheng Deng[+], Dr. Sami Malola, Woonhyuk Baek, Prof. Hannu Häkkinen,* Prof. Nanfeng Zheng,* and Prof. Taeghwan Hyeon*

[*] Dr. M. S. Bootharaju,[+] S. Lee,[+] W. Baek, Prof. T. Hyeon
Center for Nanoparticle Research, Institute for Basic Science (IBS), School of Chemical and Biological Engineering, and Institute of Chemical Processes, Seoul National University, Seoul 08826, Republic of Korea Department
E-mail: thyeon@snu.ac.kr

G. C. Deng,[+] Prof. N. F. Zheng
State Key Laboratory for Physical Chemistry of Solid Surfaces, Collaborative Innovation Center of Chemistry for Energy Materials, and Department of Chemistry, College of Chemistry and Chemical Engineering, Xiamen University, Xiamen 361005, China
E-mail: nfzheng@xmu.edu.cn

Dr. S. Malola, Prof. H. Hakkinen
Departments of Physics and Chemistry, Nanoscience Center, University of Jyväskylä, FI-40014 Jyväskylä, Finland
E-mail: hannu.j.hakkinen@jyu.fi

[+] These authors contributed equally to this work.

Supporting information for this article is given via a link at the end of the document.

Abstract: Although atomically precise metalloid nanoclusters (NCs) of identical size with distinctly different molecular structures are highly desirable to understand the structural effects on the intriguing optical and photophysical properties, their synthesis remains highly challenging. Herein, we employed phosphine and thiol capping ligands featuring appropriate steric effects and synthesized a charge-neutral Ag NC with the formula, $Ag_{44}(EBT)_{26}(TPP)_4$ (EBT: 2-ethylbenzenethiolate; TPP: triphenylphosphine). The single-crystal X-ray structure reveals that this NC has a hollow metal core of $Ag_{12}@Ag_{20}$ and a metal-ligand shell of $Ag_{12}(EBT)_{26}(TPP)_4$. The presence of mixed ligands and long V-shaped metal-ligand motifs on this NC has resulted in the enhancement of NIR-II photoluminescence quantum yield by >25-folds compared to an all-thiolate-stabilized anionic $[Ag_{44}(SR)_{30}]^{4-}$ NC (SR: thiolate). Time-dependent density functional calculations show that our Ag_{44} NC is an 18-electron superatom with a modulated electronic structure as compared to the $[Ag_{44}(SR)_{30}]^{4-}$ anion, significantly influencing its optical properties.

Introduction

Ligand-protected metalloid nanoclusters (NCs),[1] representing a new class of functional nanomaterials with a precise metal- and ligand-count, have attracted tremendous attention for not only their aesthetic atomic arrangements but also for the fascinating optical, photophysical and chemical properties.[2] The intermediate size (typically, <2 nm) of NCs bridges the gap between two different size regimes of widely explored materials, such as plasmonic metal nanoparticles (diameter >3 nm) and simple metal-ligand complexes.[2b, 3] Thus, the synthesis of a library of discrete-sized NCs will offer unprecedented opportunities to systematically study the evolution of properties of materials, such as the transition of non-metallic to metallic state, bonding at the metal-ligand interface and stability.[2b, 4] Furthermore, the NCs promise potential applications in catalysis,[5] optoelectronics,[6] energy conversion[7] and bioimaging.[8] The coinage metals (Au, Ag and Cu)[3, 9] and main group metals[10] have largely been explored for synthesizing NCs comprising tens to hundreds of metal atoms.[11]

The bottom-up approach involving chemical reduction of metal-ligand complexes in solutions is a common and straightforward synthetic strategy for a majority of the reported noble metal NCs, where the capping ligands are found to play a critical role in controlling the size and structure of NCs.[4a, 12] Particularly, the alkyl groups and their position (with respect to metal binding site) on the aromatic ring of the ligand are found to have a profound influence, which often dictate the size and structure of NCs.[12a, 13] Typical ligands used for stabilizing NCs are thiols,[14] phosphines,[15] hydrides,[16] alkynes[17] and/or their combinations.[5b, 12b] Post synthetic ligand-exchange has also been found to result in the NCs of novel size and molecular structure.[18] Recently, metals[19] and ligands[17, 20] are found to assist the synthesis of NCs without being present in the final product. Although it is highly challenging to understand the exact role of metals and ligands that mediate the synthesis of NCs, they are anticipated to form suitable intermediates, directing or facilitating the formation of NCs.

The size- and structure-property relationships in NCs are highly desirable to design NC-based materials for prospective applications in catalysis and energy conversion, which requires well-controlled size, composition, electronic charge and geometric and electronic structure.[12b, 21] Unfortunately, there are no hard and fast rules to attain NCs of desired characteristics since the molecular mechanism of the formation of NCs is still unknown. As a result, NCs of different metals with identical size, as well as NCs of the same metal with identical size but different atomic arrangements are rarely observed,[22] preventing the thorough exploration of fundamental aspects of NCs, such as size- and structure-dependencies on the optical, catalytic and photophysical properties. The $[Ag_{44}(SR)_{30}]^{4-}$ NC (SR: thiolate) is one of the early discoveries in thiolated Ag NCs,[1b, 23] which exhibits multiple absorption features in the entire UV-vis window. Its structure comprises a Ag_{32} core protected by six equivalent $Ag_2(SR)_5$ motifs. Synthesizing NCs analogues to this size and

10.1002/anie.202015907

structure would be very interesting. While there are some main-group metalloid NCs possessing the same core and different surface structures,[24] those of noble metal-based remain unavailable due to synthetic challenges, restricting the studies of surface-structure effects on their properties.

In this work, we report on the synthesis of a Ag NC by the combined use of a phosphine (triphenylphosphine, TPP) and a thiol (2-ethylbenzenethiol, EBTH) ligand with a bulky alkyl group adjacent to sulfur binding site. In the presence of a Cu source, Ag and these ligands together produce a novel $Ag_{44}(EBT)_{26}(TPP)_4$ NC, which is much desired and analogous to the reported $[Ag_{44}(SR)_{30}]^{4-}$ NC[1b, 23] in terms of total metal and ligand number. The X-ray crystal structure shows that our Ag_{44} has the metal core similar to $[Ag_{44}(SR)_{30}]^{4-}$, however with a vividly different surface structure, making $Ag_{44}(EBT)_{26}(TPP)_4$ a promising candidate for the investigation of structure-dependency on the properties of NCs. Interestingly, despite similarities in the core structures, the optical properties are completely modified due to alterations in the electronic structure as described here by time-dependent density functional theory (TDDFT) results. Furthermore, the $Ag_{44}(EBT)_{26}(TPP)_4$ NCs exhibit enhanced near-infrared-II (NIR-II, 1000-1700 nm) photoluminescence (PL).

Results and Discussion

The synthesis of $Ag_{44}(EBT)_{26}(TPP)_4$ NCs is described in the experimental section and Figure S1 in Supporting Information (SI). Briefly, Ag and Cu precursors along with tetraphenylphosphonium tetraphenylborate are reacted with EBTH in THF to form metal-thiolates. Upon addition of TPP, insoluble metal-thiolates are solubilized by complexation with TPP. Subsequently, borohydride reduction of these metal-ligand complexes has produced $Ag_{44}(EBT)_{26}(TPP)_4$ NCs. Thoroughly washed final product of NCs is dissolved in DCM and layered with *n*-hexane at 4 °C, resulting black rectangular single-crystals (Figure S2) of appropriate quality, which are used for single-crystal X-ray diffraction (SCXRD) to determine the molecular structure of NCs.

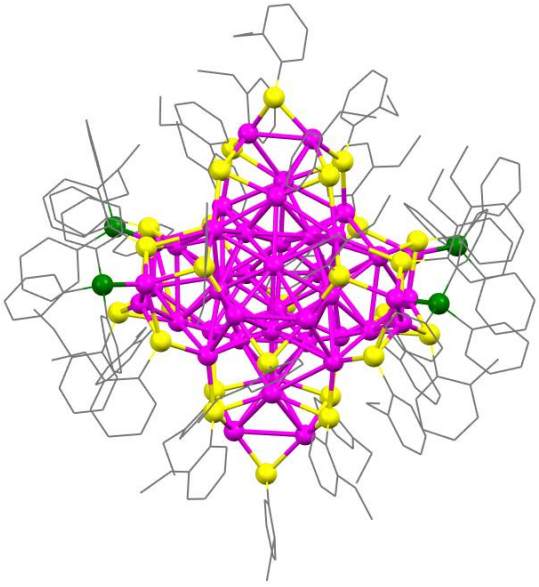

Figure 1. Total structure of $Ag_{44}(EBT)_{26}(TPP)_4$ NC determined by SCXRD. Color labels: magenta = Ag; yellow = S; green = P; gray = C. Hydrogen atoms of the ligands are not displayed for clarity.

The SCXRD analysis of a suitable single-crystal reveals that the synthesized NC consists of 44 Ag atoms and 26 EBT and four TPP ligands (Figure 1).[25] No counterions are located in the molecular structure, indicating that its electronic charge is zero. Thus, the chemical formula of the NCs determined through the SCXRD is $Ag_{44}(EBT)_{26}(TPP)_4$. The number of metal atoms and ligands is identical to that of an all-thiolate-protected Ag NC of $[Ag_{44}(SR)_{30}]^{4-}$,[23b] wherein four thiolates of $[Ag_{44}(SR)_{30}]^{4-}$ are substituted by four phosphines and the 4— charge is switched to zero. The packing structure shows that its unit cell accommodates two NCs (Figure S3) in contrast to one NC in the unit cell of $[Ag_{44}(SR)_{30}]^{4-}$ with four counterions.[23b] The $Ag_{44}(EBT)_{26}(TPP)_4$ NC is found to crystallize in a triclinic system with a space group of *P*-1 (Table S1 in SI).

A detailed structural analysis of the $Ag_{44}(EBT)_{26}(TPP)_4$ NC shows the presence of a non-centered Ag_{12} icosahedron inner core (Figure 2A). Subsequently, an Ag_{20} dodecahedron (magenta layer) completely encapsulates this Ag_{12} icosahedron to form an Ag_{32} ($Ag_{12}@Ag_{20}$) metal core (Figure 2B). There are two types of surface motifs on this NC (Figure 2C): (i) simple ligand motifs (bridging thiolates) and (ii) metal-ligand motifs (three-dimensional $Ag_2(EBT)_5$ and long V-shaped $Ag_4(EBT)_7(TPP)_2$)). Binding of these motifs with the surface of the Ag_{32} metal core, such that two of each type are positioned oppositely, generates the total structure of $Ag_{44}(EBT)_{26}(TPP)_4$ NC with a large box-like shape (Figure 2D).

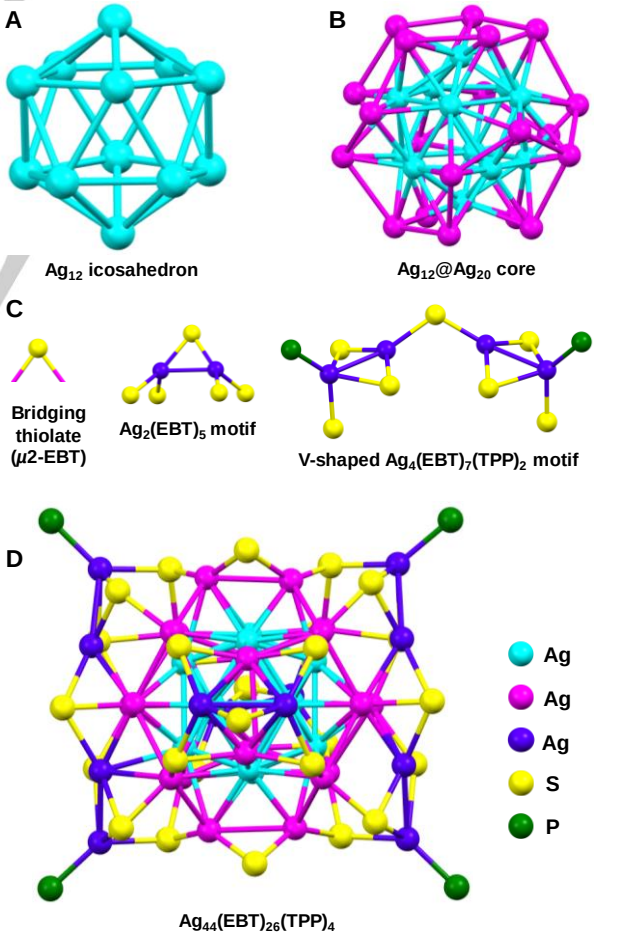

Figure 2. Structural anatomy of $Ag_{44}(EBT)_{26}(TPP)_4$ NC. (A) Ag_{12} icosahedron inner core and (B) Ag_{20} dodecahedron (magenta) encapsulating Ag_{12} inner core, producing the Ag_{32} metal core. (C) Three types of ligand and metal-ligand motifs. (D) Mounting of these motifs on the Ag_{32} core forms the complete structure of NC. Carbon atoms of the ligands are not shown for a better visualization of the structure.

10.1002/anie.202015907

It is very important to compare the structural features of $Ag_{44}(EBT)_{26}(TPP)_4$ NC with those of $[Ag_{44}(SR)_{30}]^{4-}$ NC to understand their effect on the optical properties. Notably, both the NCs share the same metal core of $Ag_{12}@Ag_{20}$ with a non-centered icosahedron inner core. However, upon close inspection, the distinct differences are apparent. The Ag-Ag bonds of Ag_{12} inner core and its encapsulating layer (Ag_{20} dodecahedron) of $Ag_{44}(EBT)_{26}(TPP)_4$ NC are significantly elongated (Table S2) with a range of 2.755-2.980 and 2.951-3.887 Å, respectively, compared to those of $[Ag_{44}(SR)_{30}]^{4-}$ NC (2.805-2.870 and 3.078-3.262 Å, respectively, Table S3). Such a large distribution of longer metal-metal bonds clearly indicates the critical role of ligands in distorting the Ag_{32} metal core of $Ag_{44}(EBT)_{26}(TPP)_4$ NC.

Note that the EBT ligand comprises a bulky ethyl group adjacent to S binding site. Ultimately, EBT ligands have to stabilize the overall NC along with the secondary TPP ligands by overcoming the intrinsic steric constraints. As a result, not only the metal core would have been distorted to accommodate EBT ligands but also modified the surface structure through two different types of ligand and metal-ligand motifs (Figure 2C). Recall that the $[Ag_{44}(SR)_{30}]^{4-}$ NC has only one-type of six $Ag_2(SR)_5$ metal-ligand motifs due to the absence of any secondary ligands, imparting more spherical nature to this cluster, whereas the $Ag_{44}(EBT)_{26}(TPP)_4$ NC appears as a box (Figure 2D) mainly due to long V-shaped $Ag_4(EBT)_7(TPP)_2$ motifs. The Ag-S bond length range for $Ag_{20\ layer}$-S in $Ag_{44}(EBT)_{26}(TPP)_4$ NC is 2.446-2.960 Å, showing the elongated Ag-S bonds compared to those (2.539-2.674 Å) of $[Ag_{44}(SR)_{30}]^{4-}$ NC. The TPP ligands are a part of V-shaped metal-ligand motifs with a Ag-P bond length range of 2.388-2.412 Å.

The molecular formula of the $Ag_{44}(EBT)_{26}(TPP)_4$ NCs obtained from the SCXRD is further supported by various characterization techniques. The matrix-assisted laser desorption ionization mass spectrometry of single crystals (Figure S4) shows a high-mass peak at ~8.3 kDa corresponding to $Ag_{44}(EBT)_{26}$, indicating the loss of TPP ligands during the ionization process. Due to the weak binding of labile ligands such as phosphines, they are detached from the cluster surface in the gas phase, which is a common observation in the mass spectrometry of noble metal NCs.[26] Nevertheless, the presence of TPP has been unambiguously confirmed by the solution-state ^1H and ^{31}P nuclear magnetic resonance (NMR) spectroscopy (Figures S5,S6). A clear shift and broadening of ^{31}P NMR peak of the NCs, compared to pristine TPP, confirm the binding of TPP with the NCs.[26] ^1H NMR spectroscopy substantiated the presence of not only TPP but also EBT ligands. Furthermore, the thermogravimetric analysis (Figure S7) shows a weight loss of 49.15%, which is in good agreement with the ligand content (49.3%) of the $Ag_{44}(EBT)_{26}(TPP)_4$ NC. The observation of NCs through transmission electron microscopy (TEM) is challenging due to their small size and sensitivity to electron beam. However, it reveals the absence of any large nanoparticles, which is a characteristic of the NCs (Figure S8). The scanning TEM energy dispersive X-ray spectroscopy of aggregates of NCs shows the presence of elements of NCs, including Ag, S and P (Figure S9).

The superatom theory[27] provides a free valence electron count of 18 for $Ag_{44}(EBT)_{26}(TPP)_4$ NC, i.e., [(44 x 1) − (26 x 1) − (4 x 0)], as each Ag contributes one *s* electron and each EBT thiolate withdraws one electron and neutral phosphine does not receive any electron. DFT analysis of symmetries of several frontier orbitals confirms this picture and establishes a HOMO-LUMO gap of 0.78 eV (Figures S10,S11) at the PBE level (see computational details in the SI). The optical absorption spectrum of $Ag_{44}(EBT)_{26}(TPP)_4$ NC shows two prominent peaks at 535 and 391 nm along with a shoulder peak around 735 nm (Figure 3, black trace). For comparison, an $[Ag_{44}(EBT)_{30}]^{4-}$ NC containing solely EBT ligands is synthesized exhibiting absorption spectrum with multiple peaks at 404, 480, 528, 635, 690 and 820 nm (Figure 3, red trace), which matches exactly with the reported $[Ag_{44}(SR)_{30}]^{4-}$ NCs.[1b, 23b] These spectra clearly suggest that the electronic structure of $Ag_{44}(EBT)_{26}(TPP)_4$ NC is strongly modified due to distortions in the metal core and differences in the molecular structure.

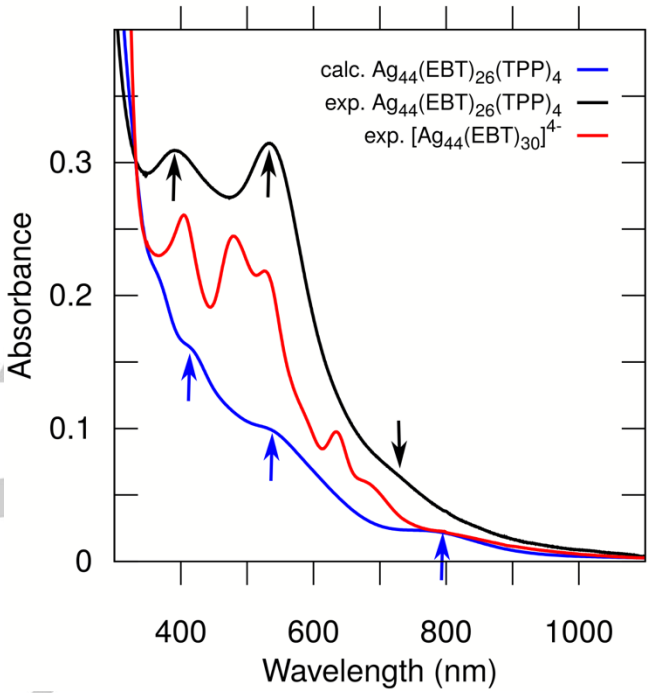

Figure 3. Experimental (black curve) and DFT calculated (blue curve) optical absorption spectra of $Ag_{44}(EBT)_{26}(TPP)_4$ NC compared with the experimental spectrum of $[Ag_{44}(EBT)_{30}]^{4-}$ NC (red curve). Arrows denote the peaks observed in calculated and experimental spectra of $Ag_{44}(EBT)_{26}(TPP)_4$ NC. The peaks in the calculated spectrum are analyzed in Figure 4.

To understand the experimental observations, we performed TDDFT calculations and analyzed the computed absorption spectrum of $Ag_{44}(EBT)_{26}(TPP)_4$ (technical details are in the SI). As shown in Figure 3, the computed spectrum (blue trace) is in a rather good agreement with the experimental data, showing peaks at 415, 530 and 775 nm (as compared to previously mentioned experimental peaks at 391, 535 and 735 nm). We analyzed the computed absorption peaks by using the so-called transition contribution maps (TCMs) (Figure 4). A corresponding analysis was done by some of us also in 2013 for the first all-thiolate protected $[Ag_{44}(SR)_{30}]^{4-}$.[23b] The lowest-energy peak of $Ag_{44}(EBT)_{26}(TPP)_4$ at 775 nm has contributions both from the superatom 1D → 1F transition and from ligand-to-metal transitions (Figure 4A), while in the case of $[Ag_{44}(SR)_{30}]^{4-}$ the peak consisted solely of superatom 1D → 1F. Transition-induced hole and electron density (Figure 4B) confirms transfer of electrons in ligands to metal core as well. The peak at 530 nm has contributions from superatom 1D → ligand states, particularly to pi-electrons of the phenyl rings in phosphine ligands (Figures 4C, 4D), and the peak at 415 nm has solely ligand-to-ligand transitions (Figures 4E, 4F).

Comparison of the electronic ground state of $Ag_{44}(EBT)_{26}(TPP)_4$ with that of the $[Ag_{44}(SR)_{30}]^{4-}$ shows that while the calculated HOMO-LUMO energy gap is very similar in both the clusters, the mixed EBT-TPP ligand layer lowers the

symmetry of the electronic state distributions. This shows up particularly in the broader dispersion of the empty 1F orbitals: Figure S10 shows that each of the seven 1F states is split in energy, while in the $[Ag_{44}(SR)_{30}]^{4-}$ case[23b] the seven states are grouped in 3, 1, 3 manifolds. Another qualitative difference is that the LUMO state of $Ag_{44}(EBT)_{26}(TPP)_4$ is of dominantly 1F symmetry, while in $[Ag_{44}(SR)_{30}]^{4-}$ it is 2S.

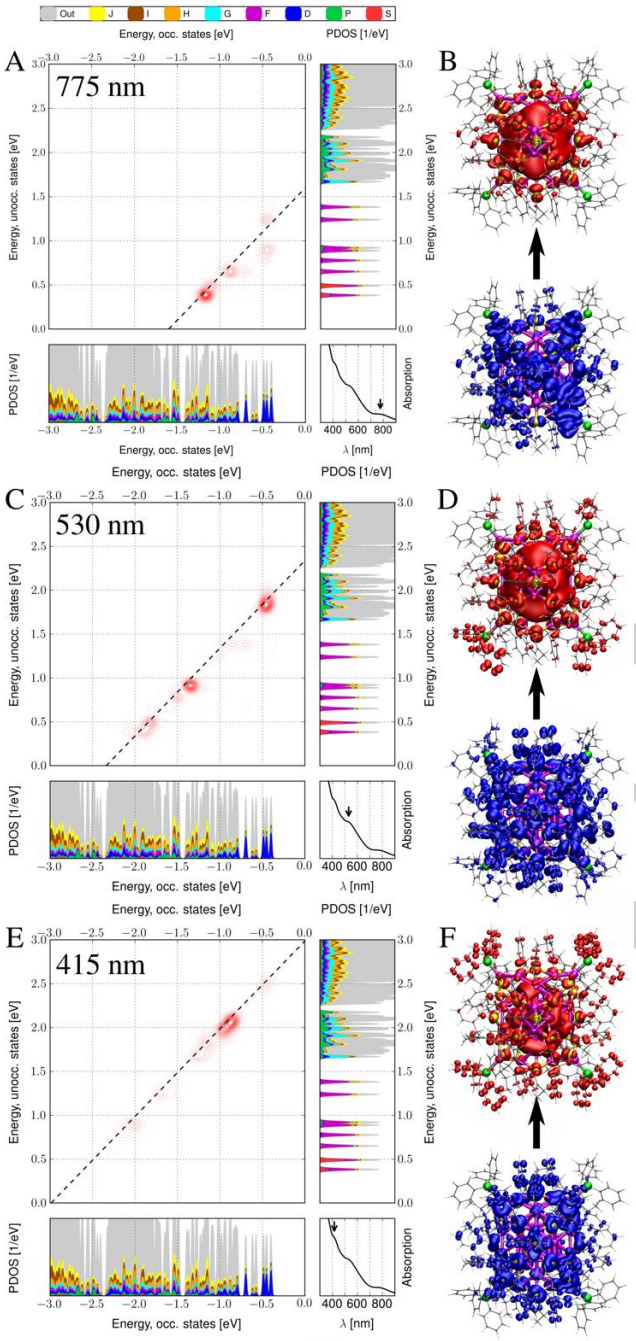

Figure 4. Analysis of the computed optical spectrum of $Ag_{44}(EBT)_{26}(TPP)_4$. Panels (A, C, and E) show the transition contribution maps (TCMs) for peaks at 775, 530 and 415 nm, respectively, and panels (B, D, and F) show the corresponding transition-induced hole-electron densities. In each TCM panel, the horizontal and vertical PDOS panels show the occupied and unoccupied Kohn-Sham electronic density of states as projected to spherical harmonics according to the color labels on top of the Figure. In the map, the contributions of the single transitions to the absorption (marked peak on the lower right corner) are shown by the red contours (high density of contours showing the higher weights).

Next, we investigate the structural effects of Ag_{44} NCs on their photophysical properties. The PL emission spectrum of $Ag_{44}(EBT)_{26}(TPP)_4$ NCs displays two broad NIR-II peaks centered at ~1124 and ~1270 nm along with another broad feature spread in the 1400-1600 nm region (Figure 5). The prominent PL peaks are blue-shifted from those of $[Ag_{44}(EBT)_{30}]^{4-}$ NCs. This may be due to the qualitative differences in the spread and nature of the frontier orbitals in these two clusters as discussed above. The prominent emission peaks of $Ag_{44}(EBT)_{26}(TPP)_4$ NCs are likely due to electron relaxation between molecular orbitals different from HOMO and LUMO, while the low-energy emission might originate from HOMO-LUMO transitions.[23b, 28] The PL excitation spectrum for emission at ~1270 nm well matches with the absorption spectrum (Figure S12), indicating the origin of the PL from the NCs. Furthermore, the PL quantum yield (PLQY) of $Ag_{44}(EBT)_{26}(TPP)_4$ is found to be ~0.26%, which is enhanced by >25- and >10-folds compared to the reported $[Ag_{44}(SR)_{30}]^{4-}$ (~0.01%)[1b] and $[Ag_{44}(EBT)_{30}]^{4-}$ (~0.02%), respectively. Importantly, the PLQY of $Ag_{44}(EBT)_{26}(TPP)_4$ is >5-folds higher compared to that of the standard dye IR26 (0.05%) and also comparable to PLQY of cyclodextrin-protected gold NCs (~0.11%).[29] The increase of PLQY of $Ag_{44}(EBT)_{26}(TPP)_4$ NCs is attributed to the presence of secondary TPP ligands, which are known to play important role in the PL enhancement of the metal NCs.[30] In addition, the rigidification of the cluster surface through interligand interactions (pi-pi stacking of EBT ligands) (Figure S13) and the presence of two long V-shaped metal-ligand motifs would have resulted in the PL enhancement.[2a, 21a]

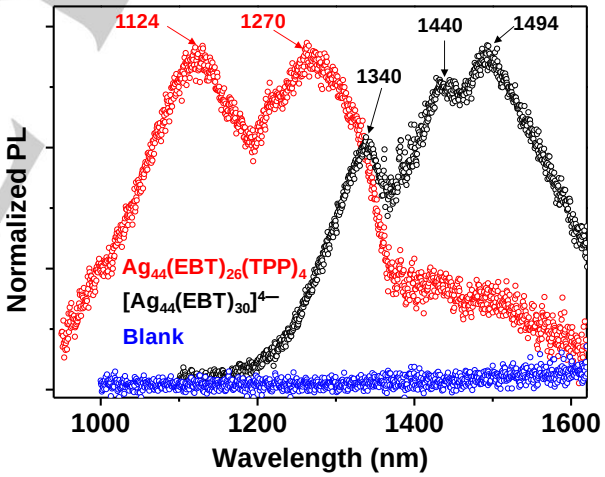

Figure 5. NIR-II PL emission spectra of $Ag_{44}(EBT)_{26}(TPP)_4$ and $[Ag_{44}(EBT)_{30}]^{4-}$ NCs and solvent (blank, dimethylformamide) collected for optical excitations at 535 nm.

We note the absence of Cu in the $Ag_{44}(EBT)_{26}(TPP)_4$ NC (Figure 1 and Table S4) although the Cu precursor $Cu(acac)_2$ (acac: acetylacetonate) is used during the synthesis of this NC. The product synthesized in the absence of Cu source shows an absorption spectrum (Figure S14A) with a broad single peak at ~447 nm corresponding to typical plasmonic Ag nanoparticles (Figure S14B), indicating that Cu is necessary for the synthesis of $Ag_{44}(EBT)_{26}(TPP)_4$ NCs in our experimental conditions. It has been observed that Pd and Cu assist the synthesis of Ag_{33} and Ag_{23} NCs, respectively.[19] However, the exact mechanism of the metal-mediated formation of NCs is still unknown due to challenges in the characterization of the atomic structures and

compositions of the reaction intermediates. The Cu is also shown to cause the size-transformation of Au NCs from Au_{25} to Au_{44}.[31]

A series of experiments was performed to understand the formation pathway of $Ag_{44}(EBT)_{26}(TPP)_4$ NCs. Time-dependent absorption spectroscopy and elemental analysis suggest that the $Ag_{44}(EBT)_{26}(TPP)_4$ NCs are formed through intermediates of AgCu alloy NCs (Figures S15-S17 and Table S4). Given the unfavorable steric and stability constraints for AgCu NCs under our reaction conditions, they would have transformed to thermodynamically and electronically stable $Ag_{44}(EBT)_{26}(TPP)_4$ NCs. Thus released Cu species would further combine with Ag to form byproducts of insoluble Ag-rich, AgCu nanoparticles and soluble AgCu/Cu-ligand complexes, which are discarded during the purification (see experimental section in the SI for details) of Ag_{44} NCs (Figures S18,S19 and Table S4). However, the yield of the $Ag_{44}(EBT)_{26}(TPP)_4$ NCs is still ~52% (Ag atom basis).

The effect of anion of the Cu source (acac) on the formation of $Ag_{44}(EBT)_{26}(TPP)_4$ NCs is found to be absent because the use of $CuCl_2$ has resulted the NC with the same absorption features (Figure S20). Nevertheless, the precise compositional and structural details of the intermediates of AgCu alloy NCs along with a detailed computational study are indeed necessary to gain molecular-level mechanistic insights into the formation of pure Ag_{44} NCs, which is beyond the scope of this work. The generality of our synthetic approach to obtain Ag_{44} or a different-size solely Ag NC is further verified by replacing the Cu source with that of Au. Surprisingly, the synthesized product is not a pure Ag NC, but is an AgAu alloy NC exhibiting NIR emission features, which are blue-shifted from those of $Ag_{44}(EBT)_{26}(TPP)_4$ NCs (Figures S21,S22). This indicates that our method is specific to Cu for Ag_{44} synthesis. Furthermore, for the metal combination Ag and Cu, different thiols such as 1,3-benzenedithiol and 2,4-dichlorobenzenethiol provide AgCu alloy NCs, $Ag_{17}Cu_{12}$ and $Ag_{28}Cu_{12}$, respectively.[32] These experimental results together establish that the choice of ligands and metals plays crucial role in obtaining NCs of specific size, structure and composition.

Conclusion

In conclusion, by judicious choice of an aromatic thiol, containing a bulky alkyl group adjacent to sulfur binding site, and a phosphine coligand, a silver nanocluster $Ag_{44}(EBT)_{26}(TPP)_4$ is synthesized and its single crystal X-ray structure is determined. Its core structure ($Ag_{12}@Ag_{20}$) resembles that of well-known $[Ag_{44}(SR)_{30}]^{4-}$ cluster, while the surface structure is different, since four negative thiolates of $[Ag_{44}(SR)_{30}]^{4-}$ are replaced by four neutral phosphines. Significant distortions in the metal core as well as novel surface structure of our nanocluster are found to significantly modify the electronic structure and optical properties. Furthermore, the presence of phosphine and rigidified surface through interligand interactions have resulted in the enhancement of NIR-II photoluminescence quantum yield by >25-folds. The TDDFT calculations revealed important differences in the details of the electronic structure of $Ag_{44}(EBT)_{26}(TPP)_4$ as compared to the previously documented $[Ag_{44}(SR)_{30}]^{4-}$ which underlie the observed photophysical properties. We hope that these two Ag_{44} nanoclusters of identical size and different molecular structures will enable researchers to conduct more fundamental studies to understand the structure-property relationships.

Acknowledgements

T.H. acknowledges the financial support by the Research Center Program of the IBS (IBS-R006-D1) in Korea. The computational work at University of Jyväskylä was supported by the Academy of Finland (grants 292352, 294217, and 319208). N.F.Z. thanks the National Key R&D Program of China (2017YFA0207304) and the NSF of China (21890752, 21731005, 21721001) for financial support.

Conflict of interest

The authors declare no conflict of interest.

Keywords: silver • nanoclusters • single crystal X-ray structure • NIR-II photoluminescence • superatom

[1] a) M. Zhou, T. Higaki, G. Hu, M. Y. Sfeir, Y. Chen, D.-e. Jiang, R. Jin, *Science* **2019**, *364*, 279-282; b) O. M. Bakr, V. Amendola, C. M. Aikens, W. Wenseleers, R. Li, L. Dal Negro, G. C. Schatz, F. Stellacci, *Angew. Chem. Int. Ed.* **2009**, *48*, 5921-5926.

[2] a) L. He, Z. Gan, N. Xia, L. Liao, Z. Wu, *Angew. Chem. Int. Ed.* **2019**, *58*, 9897-9901; b) I. Chakraborty, T. Pradeep, *Chem. Rev.* **2017**, *117*, 8208-8271; c) E. Khatun, P. Chakraborty, B. R. Jacob, G. Paramasivam, M. Bodiuzzaman, W. A. Dar, T. Pradeep, *Chem. Mater.* **2020**, *32*, 611-619.

[3] a) K. L. D. M. Weerawardene, P. Pandeya, M. Zhou, Y. Chen, R. Jin, C. M. Aikens, *J. Am. Chem. Soc.* **2019**, *141*, 18715-18726; b) X. Ma, Y. Bai, Y. Song, Q. Li, Y. Lv, H. Zhang, H. Yu, M. Zhu, *Angew. Chem. Int. Ed.* **2020**, *59*, 17234-17238.

[4] a) X. Kang, Y. Li, M. Zhu, R. Jin, *Chem. Soc. Rev.* **2020,** *49*, 6443-6514; b) X. Liu, J. Chen, J. Yuan, Y. Li, J. Li, S. Zhou, C. Yao, L. Liao, S. Zhuang, Y. Zhao, H. Deng, J. Yang, Z. Wu, *Angew. Chem. Int. Ed.* **2018**, *57*, 11273-11277; c) Q. Tang, G. Hu, V. Fung, D.-e. Jiang, *Acc. Chem. Res.* **2018**, *51*, 2793-2802.

[5] a) T. Higaki, Y. Li, S. Zhao, Q. Li, S. Li, X.-S. Du, S. Yang, J. Chai, R. Jin, *Angew. Chem. Int. Ed.* **2019**, *58*, 8291-8302; b) S. Lee, M. S. Bootharaju, G. Deng, S. Malola, W. Baek, H. Häkkinen, N. Zheng, T. Hyeon, *J. Am. Chem. Soc.* **2020**, *142*, 13974-13981.

[6] P. Chakraborty, A. Nag, K. S. Sugi, T. Ahuja, B. Varghese, T. Pradeep, *ACS Mater. Lett.* **2019**, *1*, 534-540.

[7] Y. Wang, X.-H. Liu, Q. Wang, M. Quick, S. A. Kovalenko, Q.-Y. Chen, N. Koch, N. Pinna, *Angew. Chem. Int. Ed.* **2020**, *59*, 7748-7754.

[8] S. Shahsavari, S. Hadian-Ghazvini, F. Hooriabad Saboor, I. Menbari Oskouie, M. Hasany, A. Simchi, A. L. Rogach, *Mater. Chem. Front.* **2019**, *3*, 2326-2356.

[9] a) J.-Y. Liu, F. Alkan, Z. Wang, Z.-Y. Zhang, M. Kurmoo, Z. Yan, Q.-Q. Zhao, C. M. Aikens, C.-H. Tung, D. Sun, *Angew. Chem. Int. Ed.* **2019**, *58*, 195-199; b) R.-W. Huang, J. Yin, C. Dong, A. Ghosh, M. J. Alhilaly, X. Dong, M. N. Hedhili, E. Abou-Hamad, B. Alamer, S. Nematulloev, Y. Han, O. F. Mohammed, O. M. Bakr, *J. Am. Chem. Soc.* **2020**, *142*, 8696-8705; c) X. Kang, M. Zhu, *ACS Mater. Lett.* **2020**, *10*, 1303–1314; d) M. J. Alhilaly, R.-W. Huang, R. Naphade, B. Alamer, M. N. Hedhili, A.-H. Emwas, P. Maity, J. Yin, A. Shkurenko, O. F. Mohammed, M. Eddaoudi, O. M. Bakr, *J. Am. Chem. Soc.* **2019**, *141*, 9585-9592.

[10] a) A. Schnepf, H. Schnöckel, *Angew. Chem. Int. Ed.* **2001**, *40*, 711-715; b) A. Ecker, E. Weckert, H. Schnöckel, *Nature* **1997**, *387*, 379-381; c) M. Binder, C. Schrenk, A. Schnepf, *Chem. Commun.* **2019**, *55*, 12148-12151.

[11] a) T. I. Levchenko, C. Kübel, B. Khalili Najafabadi, P. D. Boyle, C. Cadogan, L. V. Goncharova, A. Garreau, F. Lagugné-Labarthet, Y. Huang, J. F. Corrigan, *J. Am. Chem. Soc.* **2017**, *139*, 1129-1144; b) D. R. Kauffman, D. Alfonso, D. N. Tafen, J. Lekse, C. Wang, X. Deng, J. Lee, H. Jang, J.-s. Lee, S. Kumar, C. Matranga, *ACS Catal.* **2016**, *6*, 1225-1234.

[12] a) L. He, J. Yuan, N. Xia, L. Liao, X. Liu, Z. Gan, C. Wang, J. Yang, Z. Wu, *J. Am. Chem. Soc.* **2018**, *140*, 3487-3490; b) T. Kawawaki, Y. Mori, K. Wakamatsu, S. Ozaki, M. Kawachi, S. Hossain, Y. Negishi, *J. Mater.*

Chem. A **2020**, *8*, 16081-16113; c) I. Chakraborty, W. Kurashige, K. Kanehira, L. Gell, H. Häkkinen, Y. Negishi, T. Pradeep, *J. Phys. Chem. Lett.* **2013**, *4*, 3351-3355.

[13] Y. Chen, C. Zeng, D. R. Kauffman, R. Jin, *Nano Lett.* **2015**, *15*, 3603-3609.

[14] a) M. Bodiuzzaman, A. Ghosh, K. S. Sugi, A. Nag, E. Khatun, B. Varghese, G. Paramasivam, S. Antharjanam, G. Natarajan, T. Pradeep, *Angew. Chem. Int. Ed.* **2019**, *58*, 189-194; b) S. K. Barik, T.-H. Chiu, Y.-C. Liu, M.-H. Chiang, F. Gam, I. Chantrenne, S. Kahlal, J.-Y. Saillard, C. W. Liu, *Nanoscale* **2019**, *11*, 14581-14586.

[15] X. Yuan, C. Sun, X. Li, S. Malola, B. K. Teo, H. Häkkinen, L.-S. Zheng, N. Zheng, *J. Am. Chem. Soc.* **2019**, *141*, 11905-11911.

[16] R. S. Dhayal, W. E. van Zyl, C. W. Liu, *Acc. Chem. Res.* **2016**, *49*, 86-95.

[17] M. Qu, H. Li, L.-H. Xie, S.-T. Yan, J.-R. Li, J.-H. Wang, C.-Y. Wei, Y.-W. Wu, X.-M. Zhang, *J. Am. Chem. Soc.* **2017**, *139*, 12346-12349.

[18] X. Kang, M. Zhu, *Chem. Mater.* **2019**, *31*, 9939-9969.

[19] a) F. Tian, R. Chen, *J. Am. Chem. Soc.* **2019**, *141*, 7107-7114; b) X. Lin, C. Liu, X. Fu, J. Huang, *Chem. Asian J.* **2019**, *14*, 972-976.

[20] M. S. Bootharaju, H. Chang, G. Deng, S. Malola, W. Baek, H. Häkkinen, N. Zheng, T. Hyeon, *J. Am. Chem. Soc.* **2019**, *141*, 8422-8425.

[21] a) Y. Chen, M. Zhou, Q. Li, H. Gronlund, R. Jin, *Chem. Sci.* **2020**, *11*, 8176-8183; b) B. Kumar, T. Kawawaki, N. Shimizu, Y. Imai, D. Suzuki, S. Hossain, L. V. Nair, Y. Negishi, *Nanoscale* **2020**, *12*, 9969-9979; c) T. Omoda, S. Takano, T. Tsukuda, *Small* **2020**, 2001439. d) K. Kim, K. Hirata, K. Nakamura, H. Kitazawa, S. Hayashi, K. Koyasu, T. Tsukuda, *Angew. Chem. Int. Ed.* **2019**, *58*, 11637-11641; e) W. Choi, G. Hu, K. Kwak, M. Kim, D.-e. Jiang, J.-P. Choi, D. Lee, *ACS Appl. Mater. Interfaces* **2018**, *10*, 44645-44653.

[22] a) C. P. Joshi, M. S. Bootharaju, M. J. Alhilaly, O. M. Bakr, *J. Am. Chem. Soc.* **2015**, *137*, 11578-11581; b) M. S. Bootharaju, S. M. Kozlov, Z. Cao, A. Shkurenko, A. M. El-Zohry, O. F. Mohammed, M. Eddaoudi, O. M. Bakr, L. Cavallo, J.-M. Basset, *Chem. Mater.* **2018**, *30*, 2719-2725; c) A. Schnepf, E. Weckert, G. Linti, H. Schnöckel, *Angew. Chem. Int. Ed.* **1999**, *38*, 3381-3383; d) A. Schnepf, G. Stößer, H. Schnöckel, *Angew. Chem. Int. Ed.* **2002**, *41*, 1882-1884; e) A. Schnepf, R. Köppe, E. Weckert, H. Schnöckel, *Chem. Eur. J.* **2004**, *10*, 1977-1981.

[23] a) A. Desireddy, B. E. Conn, J. Guo, B. Yoon, R. N. Barnett, B. M. Monahan, K. Kirschbaum, W. P. Griffith, R. L. Whetten, U. Landman, T. P. Bigioni, *Nature* **2013**, *501*, 399-402; b) H. Yang, Y. Wang, H. Huang, L. Gell, L. Lehtovaara, S. Malola, H. Häkkinen, N. Zheng, *Nat. Commun.* **2013**, *4*, 2422.

[24] a) A. Schnepf, *Angew. Chem. Int. Ed.* **2003**, *42*, 2624-2625; b) G. N. Reddy, R. Parida, S. Giri, *Chem. Commun.* **2017**, *53*, 13229-13232; c) C. Schrenk, F. Winter, R. Pöttgen, A. Schnepf, *Chem. Eur. J.* **2015**, *21*, 2992-2997.

[25] CCDC 2032634 contains the supplementary crystallographic data for this paper. These data can be obtained free of charge from The Cambridge Crystallographic Data Centre (CCDC).

[26] M. J. Alhilaly, M. S. Bootharaju, C. P. Joshi, T. M. Besong, A.-H. Emwas, R. Juarez-Mosqueda, S. Kaappa, S. Malola, K. Adil, A. Shkurenko, H. Häkkinen, M. Eddaoudi, O. M. Bakr, *J. Am. Chem. Soc.* **2016**, *138*, 14727-14732.

[27] M. Walter, J. Akola, O. Lopez-Acevedo, P. D. Jadzinsky, G. Calero, C. J. Ackerson, R. L. Whetten, H. Grönbeck, H. Häkkinen, *Proc. Natl. Acad. Sci.* **2008**, *105*, 9157-9162.

[28] a) X.-K. Wan, W. W. Xu, S.-F. Yuan, Y. Gao, X.-C. Zeng, Q.-M. Wang, *Angew. Chem. Int. Ed.* **2015**, *54*, 9683-9686; b) K. L. D. M. Weerawardene, C. M. Aikens, *J. Phys. Chem. C* **2018**, *122*, 2440-2447.

[29] a) S. Zhu, R. Tian, A. L. Antaris, X. Chen, H. Dai, *Adv. Mater.* **2019**, *31*, 1900321; b) X. Song, W. Zhu, X. Ge, R. Li, S. Li, X. Chen, J. Song, J. Xie, X. Chen, H. Yang, *Angew. Chem. Int. Ed*. https://doi.org/10.1002/anie.202010870.

[30] X. Kang, S. Wang, M. Zhu, *Chem. Sci.* **2018**, *9*, 3062-3068.

[31] M.-B. Li, S.-K. Tian, Z. Wu, R. Jin, *Chem. Commun.* **2015**, *51*, 4433-4436.

[32] a) X. Kang, H. Abroshan, S. Wang, M. Zhu, *Inorg. Chem.* **2019**, *58*, 11000-11009; b) J. Yan, H. Su, H. Yang, C. Hu, S. Malola, S. Lin, B. K. Teo, H. Häkkinen, N. Zheng, *J. Am. Chem. Soc.* **2016**, *138*, 12751-12754.

10.1002/anie.202015907

Entry for the Table of Contents

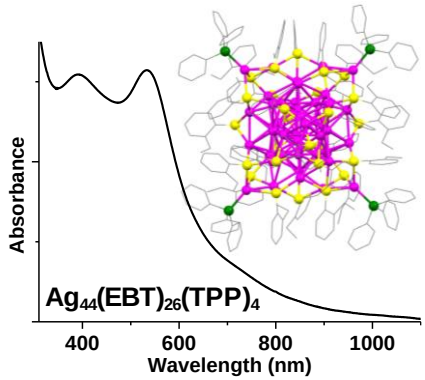

In this work, synthesis and total structure determination of a novel $Ag_{44}(EBT)_{26}(TPP)_4$ nanocluster, the first analogue of $[Ag_{44}(SR)_{30}]^{4-}$ nanocluster, are reported. The identical size and similar core- and different surface-structures of these two nanoclusters enable the study of the structural effect on the optical and photophysical properties. The novel surface structure plays crucial role in the enhancement of NIR-II photoluminescence.